RICHARD A. FARRELL, C. BRENT BARGERON, W. RICHARD GREEN, and RUSSELL L. McCALLY

COLLABORATIVE BIOMEDICAL RESEARCH ON CORNEAL STRUCTURE

The interplay between theory and experiment has led to the development of light scattering as a tool to probe the ultrastructure of the eye's cornea. This interplay has also yielded an explanation of infrared radiation damage to corneal cells.

INTRODUCTION

The cornea is the window in the wall of the eye through which we see (Fig. 1a). This highly specialized tissue must not only possess the strength necessary to withstand the intraocular pressure but must also accurately maintain its curvature because the curved air/cornea interface provides about 75% of the eye's focusing power. Understanding corneal structure is therefore important because it determines the cornea's mechanical properties and underlies the most essential characteristic of the cornea – its transparency.

The ophthalmologist's slit lamp microscope reveals that the cornea is a layered structure (Fig. 1b). At somewhat higher magnification (Fig. 1c), light microscopy allows us to see the layers in more detail. At the front is a cellular layer called the epithelium, which is about six cells thick. These cells rest on a very thin filamentous structure called the basement membrane. At the back is a single cell layer called the endothelium, which is attached to a thin collagenous layer called Descemet's membrane. The stroma occupies the region between the epithelial basement membrane and Descemet's membrane. It accounts for 90% of the corneal thickness, which is about 0.5 millimeter in humans and about 0.4 millimeter in rabbits, a common experimental animal.

The stroma is itself a layered structure. It is made up of a large number of stacked sheets, called lamellae, between which are interspersed a few flat cells. The cells, called keratocytes, occupy 3 to 5% of the corneal volume. The lamellae have relatively uniform thicknesses of approximately 2 micrometers. High magnification electron micrographs (cf. Fig. 1d) reveal that they are composed of uniform-diameter fibrils of the protein collagen surrounded by an optically homogenous macromolecular solution called the ground substance. Within a single sheet, the fibrils, which are approximately 0.025 micrometer in diameter, lie parallel to each other and to the corneal surfaces. The fibrils extend entirely across the cornea; acting much like reinforcing rods in concrete, they give the cornea its required strength. The fibril axes in adjacent lamellae make large angles with one another.

Transparency in the cornea requires that there be little or no absorption or scattering of light. It has been observed that the cornea does not absorb in the visible portion of the spectrum. The slight diminution of the intensity of visible light as it traverses a normal cornea is caused by scattering. Understanding the relationship between scattering and the corneal structure has been a major problem in ophthalmic research.[1]

The collagen fibrils are the primary scattering elements in the cornea. Because their diameter is small compared to the wavelengths of visible light and their refractive index is close to that of the ground substance, the fibrils are inefficient scatterers. However, they make up for their inefficiency by their large numbers, and a simple calculation shows that the cornea would not be transparent if the fibrils scattered independently of one another. This implies that the fibrils do not act as independent scatterers and that interference effects are therefore important in explaining the cornea's very real transparency.[1-3]

Research directed at explaining the passage of light through the multitudes of collagen fibrils has a long history at APL[2,4-6] and was the subject of an earlier *Technical Digest* article.[6] The early APL research addressed the question of whether the structures shown in electron micrographs, such as Fig. 1d, would lead to the observed transparency. A statistical analysis of the fibril positions revealed the presence of short-range order sufficient to cause the electric fields scattered from the individual fibrils to partially cancel one another by destructive interference.[2,4] Including this interference effect in the calculations led to good agreement with the measured transmissivity.
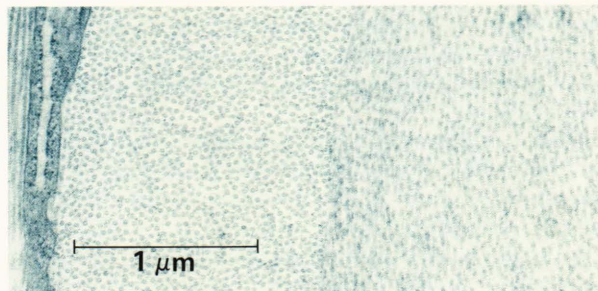
Although this approach demonstrated that the observed transparency could not be used to dismiss the
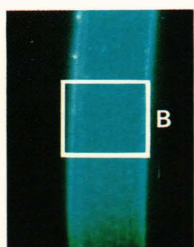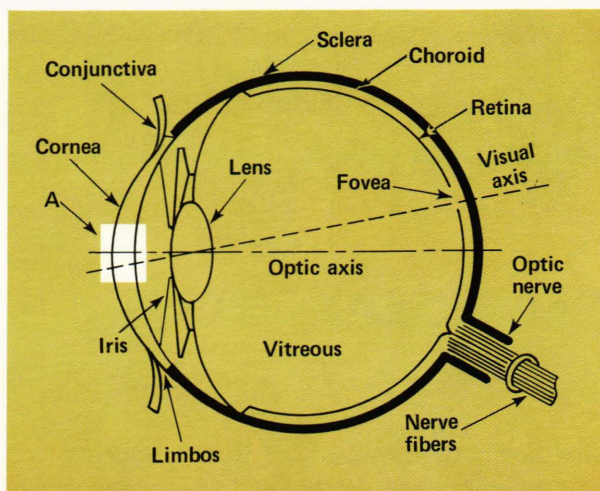
Detail A
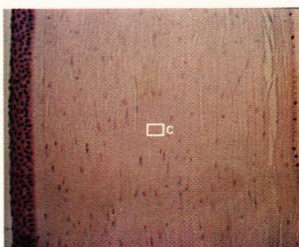
Detail B

Detail C

Figure 1 — (a) Diagram of the eye showing the location of the transparent cornea. Parts b, c, and d show the cornea in ever-increasing detail to reveal its structural elements. (b) The cornea as viewed in an ophthalmologist's slit lamp microscope. The bright bands on the front and back surfaces are, respectively, the epithelial and endothelial cell layers that bound the central stromal region. (c) A light micrograph of a cross section cut through the thickness of the cornea. At this magnification, individual epithelial and endothelial cells can be seen. This micrograph shows that the stroma is itself a layered structure and contains a few cells (keratocytes) between the layers. (d) An electron micrograph of a small region of the stroma that shows that each layer (lamella) is made up of a large number of parallel fibrils of the protein collagen. Each fibril extends entirely across the cornea; together they give the cornea the strength required to support the intraocular pressure. The fibrils in adjacent layers make large angles with one another.

fibril arrangements shown in electron micrographs, neither did it prove their validity. The problem is that the preservation, dehydration, and embedding proce-

dures required for electron microscopy could alter the detailed structure. Indeed, other investigators had dismissed the fibrillar arrangements in electron micrographs as artifacts and had proposed other structure models to explain the transparency. Two of these investigators[1,7] postulated crystalline lattice-like fibril arrangements and showed that they produced sufficient interference to be consistent with transparency. Another investigation[8] presented electron microscopic evidence of fibrils binding much more water than others had found, so that the fibril refractive index more nearly matched that of the ground substance. This matching would induce transparency by reducing scattering rather than by destructive interference.

Two other structure models were proposed to explain the increased scattering that gives swollen corneas their cloudy appearance.[9,10] Benedek and his co-workers[9,11] attributed the increase to inhomogeneities in the fibril distributions as depicted in electron micrographs. Twersky[10] showed that the increase in the volume not occupied by fibrils in a swollen cornea could explain the turbidity on the basis of a homogeneously disordered fibril distribution.

The first section of this article deals with the theoretical considerations we used to find a scattering property that could be measured in fresh (unfixed) corneas and that would allow us to distinguish among the proposed structure models. We then describe the measurements of this property (viz., the wavelength dependence of scattering) and show that the scattering is consistent with the observed electron micrographic structures. The second section of the article describes how we extended the light scattering method by including polarization effects, in order to deduce large-scale structural information, especially about the lamellar organization of the cornea. Additionally, those methods enabled us to rule out the transparency theory, which is based on nearly equal refractive indices. The third and final section of the paper reviews our research on structural alterations arising from the absorption of infrared radiation by the cornea. Most of the earlier infrared work (conducted elsewhere) concentrated on epithelial damage caused by 10.6-micrometer radiation, which is entirely absorbed within this frontmost cell layer. We have examined epithelial, stromal, and endothelial damage and in this paper discuss our research in terms of thermal damage models. The results show that all corneal cells have similar sensitivities to temperature increases.

STRUCTURAL IMPLICATIONS OF UNPOLARIZED LIGHT SCATTERING

When examining the cornea in a slit lamp microscope, the ophthalmologist is looking at the small residual light scattering that takes place in this essentially transparent tissue. As noted above, most modern theories of transparency are based on interference effects that arise because of a certain degree of

order in the spatial arrangement of collagen fibrils in the stroma. This ordering also affects the residual scattering, and we recognized that the scattering properties could, at least in principle, be used to probe corneal structure.[3,12]

Light scattering measurements are made on fresh tissues and therefore are not susceptible to artifacts that might be present in tissue prepared for electron microscopy. The measurements cannot, of course, provide a detailed ultrastructure probe because the dimensions of the relevant structures are smaller than or, at most, comparable to the light wavelength λ, being on the order of $\lambda/10$ to $\lambda/3$. Rather, our objective has been to use light scattering measurements on fresh tissues to distinguish among the various structure models that have been set forth to explain the transparency of normal corneas [1,2,4-8] and the turbidity of abnormal corneas. [9-11] We have used the wavelength dependence of scattering to demonstrate that transparency is the result of a short-range spatial ordering of the fibrils and that the increased scattering observed in swollen corneas is caused by an inhomogeneous disruption of this ordering.[3,12] The spatial arrangements shown in electron micrographs are consistent with both findings. The theoretical considerations that led us to examine the wavelength dependencies are outlined below, as are the actual experiments.

Although the details of the stromal ultrastructure depicted in electron micrographs may have been corrupted by the tissue preparation procedures, it is generally accepted that the stroma is composed of stacked sheets (lamellae), each of which contains long, thin, parallel collagen fibrils embedded in a ground substance. In general, predicting the light scattering to be expected from such an assembly would be a complicated multiple scattering problem. That is, the electric field experienced by any fibril would consist of the incident plane wave field from the light source and the scattered fields from the other fibrils. However, because the normal cornea is transparent, it is reasonable to simplify the calculations by introducing the Born approximation in which the field experienced by a fibril is approximated by the incident (plane wave) field. At a distance from the cornea that is large compared to the linear dimensions of the illuminated region, the Born approximation to the scattered electric field can be written as

$$\mathbf{E}_{sc} = \sum_{j=1}^{N} \mathbf{E}_{sc}^{(j)} \, e^{-i\mathbf{q}\cdot\mathbf{r}_j} \,. \qquad (1)$$

In this equation, N is the total number of fibrils, $\mathbf{q} = k[\mathbf{S}_1 - \mathbf{S}_0]$ with k the wavenumber $2\pi/\lambda$, and $\mathbf{S}_1$ and $\mathbf{S}_0$ are unit vectors in the scattered and incident directions, respectively. The vector $\mathbf{r}_j$ specifies the position of the jth fibril relative to some fixed origin, and $\mathbf{E}_{sc}^{(j)}$ is the field that would be scattered from the jth fibril if it were at the fixed origin. Its displacement from the origin is accounted for by the expo-

nential phase factor. The field $\mathbf{E}_{sc}^{(j)}$ depends on the diameter, refractive index, and orientation of the jth fibril and on the wavelength of the incident radiation.

For illustrative purposes, we will treat scattering by a single lamella containing N_l fibrils and assume the fibrils are identical, in which case

$$\mathbf{E}_{sc} = \mathbf{E}_0 \sum_{j=1}^{N_l} e^{-i\mathbf{q}\cdot\mathbf{r}_j} \,. \qquad (2)$$

The scattered intensity and therefore the scattering cross section, σ, are proportional to the absolute square of the field; i.e.,

$$\sigma \propto |\mathbf{E}_0|^2 \left\{ N_l + \sum_{i=1}^{N_l} \sum_{j=1}^{N_l}{}' e^{i\mathbf{q}\cdot(\mathbf{r}_j - \mathbf{r}_i)} \right\}, \qquad (3)$$

where the prime on the double sum indicates $j \neq i$. The terms for which $j = i$ have been gathered in the factor N_l.

The double sum accounts for interference among the fields scattered by different fibrils, and its value depends critically on the nature of the fibril distribution. For example, with a random assembly, the positions of the fibrils would be uncorrelated, and the double sum would vanish because the independent phase factors average to zero. For that case, the scattering cross section is simply N_l multiplied by the cross section of an isolated fibril, and the wavelength dependence is the same as that of $|\mathbf{E}_0|^2$, which is inverse cubic $(1/\lambda^3)$.[1,4]

This same wavelength dependence is predicted for distributions like those shown in electron micrographs of normal corneas, for which there is a short-range order. Short-range order means that the fibril positions about any reference fibril are correlated with one another for some short distance (a few fibril spacings).[3,4,12] For such a distribution, the interference term does not average to zero, but it can be shown that the lowest order approximation for the term in braces in Eq. 3 is μN_l. The parameter μ is the normalized mean square fluctuation (variance) in the number of fibrils in an area whose linear dimensions are large compared to a correlation length. An analysis of typical electron micrographs of healthy nonswollen corneas shows that μ is approximately 0.1; thus the scattering would be reduced to about 10% of that for the completely random distribution.

For a crystalline lattice arrangement, correlation exists at all separation distances. Because the lattice spacing (fibril separation) is small compared to the light wavelength, there would be no scattering. The interference term would equal $-N_l$, and the two terms in braces in Eq. 3 would cancel.[1] Quasi-crystalline arrangements in which there are small random displacements from the perfect lattice positions also possess long-range order. For such distributions, it is convenient to expand the interference term of Eq. 3

in a Taylor series about the ideal lattice positions. It is easy to show that the lowest order contribution equals $-N_l$, which would cancel the term in brackets, as in the perfect crystalline lattice example. The next order contribution is proportional to λ^{-2} and, as noted previsiouly, the term multiplying the brackets varies as λ^{-3}. Thus, long-range order models would lead to a scattering cross section that varied as the inverse fifth power of light wavelength.[7] Therefore, structure models having short-range and long-range order can be distinguished via light scattering experiments.[3,12]

As noted in the Introduction, models developed to explain the loss of transparency arising from the increased scattering that accompanies corneal swelling also lend themselves to similar tests. Twersky[10] "explained" this increased scattering on the basis of a hard-core model in which the collagen fibrils are coated by a material having the same refractive index as the ground substance. In such models, ordering is caused by the condition that two fibrils cannot approach each other closer than touching. Twersky fixed the effective hard-core diameter of the fibril so as to obtain sufficient short-range ordering in the fibril positions to allow agreement with the measured transmissivity of the normal cornea. He then showed that the increased volume per fibril in a cornea swollen to 1.5 times its normal thickness would induce a homogeneous disordering of the fibril arrangement sufficient to produce reasonable agreement with the measured transmissivity at a light wavelength of 0.5 micrometer. Because this homogeneous disordering only has the effect of increasing the parameter μ, a $1/\lambda^3$ dependence would be expected for the scattering.

Electron micrographs do not depict a homogeneous disordering of fibril positions; rather, they show that swelling is accompanied by the appearance of regions (called "lakes") completely void of fibrils, as shown schematically in Fig. 2a. Many workers suggested that these lakes were artifacts. Benedek and his co-workers at MIT, however, postulated that it is the presence of these voids that causes the increased light scattering that gives the swollen cornea its milky appearance.[9,11]

Benedek devised an ingenious method for taking lakes into explicit account when calculating light scattering.[9] The approach, shown in Fig. 2, is based on recognizing that the actual fibril distribution is equivalent to one in which the lakes are populated by fibrils minus a distribution consisting of the fibrils used to populate the lakes. One then calculates the fields resulting from these two distributions and keeps track of the terms resulting from the latter distribution in calculating the intensity. Quantitative calculations based on this method have not been carried out; but we were able to use it to show that the presence of lakes would add a term to the total cross section which varies as the inverse second power of wavelength and which would dominate in highly turbid corneas. Thus the scattering from such corneas should vary as λ^{-2}, a result clearly discernible by careful light scattering experiments.

We chose to measure the total scattering cross section. The process of averaging over all the lamellae and integrating over all possible scattering angles in order to compute this quantity from the cross section in Eq. 3 does not change the wavelength dependencies. The light scattering apparatus we used is shown schematically in Fig. 3.[3] The collimated light from a stabilized tungsten bulb passes through the cornea; the light transmitted within an acceptance angle of $\pm 1.5°$ is collected and filtered through a monochromator, where it is detected by a photomultiplier. The cornea is surrounded by a nutritive, balanced saline solution that maintains its physiological condition and also nearly matches its refractive index. The fraction of light transmitted by the cornea, F_T, is the ratio of the intensity transmitted when the cornea is in position to the intensity when it is removed. It is related to the total scattering cross section (per unit length) per fibril by

$$\sigma_s = [1/(\rho\Delta)]\ln F_T , \qquad (4)$$

in which ρ is the average number density of fibrils (the number of fibrils per unit area in a cross section cut through a lamella of the stroma) and Δ is the stromal thickness.
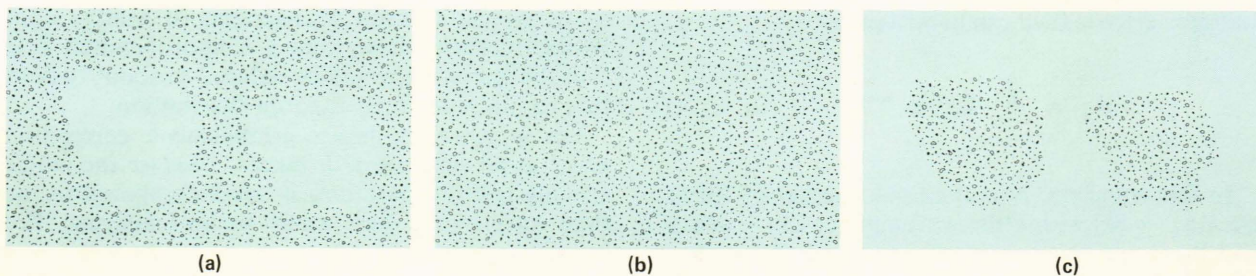

(a) (b) (c)

Figure 2 — Method of calculating the scattering from "lakes." (a) is a schematic representation of a fibril distribution that contains voids or lakes. (b) shows the same distribution with the voids filled in with fibrils of the same average number density and relative spatial distribution as the nonvoid regions of (a). (c) shows only the distribution of fibrils used to populate the voids. In the actual calculation, these fibrils are assigned negative scattering amplitudes. Thus, the field scattered by the sum of distributions (b) and (c) would be the same as that scattered by distribution (a).
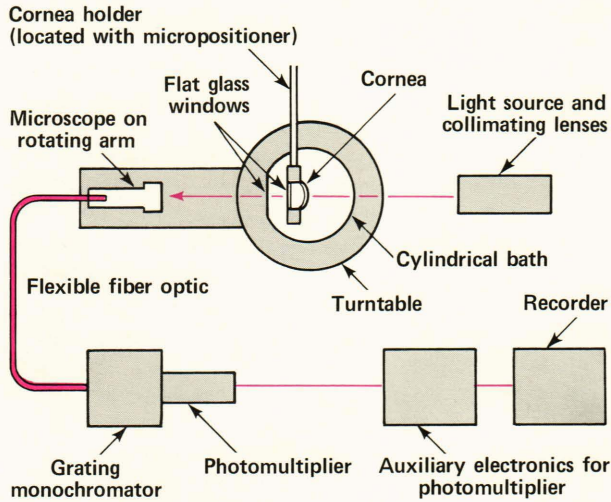
Figure 3 — A schematic view of the apparatus for measuring transmission or angular scattering as a function of light wavelength. The illuminated portion of the cornea is held fixed at the center of a cylindrical bath. The bath is mounted on a turntable, together with the collection optics. Rotation of the turntable permits measurements of the light scattered from the same portion of the cornea, independent of scattering angle.
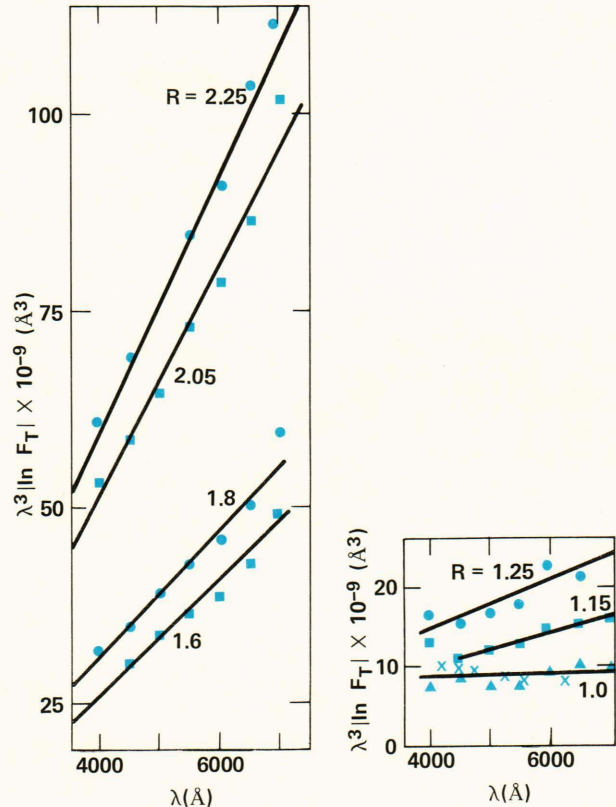

Figure 4 — The wavelength dependence of the total light scattering cross section from normal and swollen corneas. As discussed in the text, the actual quantity plotted is $\lambda^3 \langle \rho_0 \sigma_s \rangle$. Multiplication by the cube of the light wavelength removes the inverse cubic wavelength dependence that is characteristic of the individual fibril cross section. If the normal cornea scattering is from fibrils distributed with short-ranged ordering of their positions, the resulting plot would have zero slope, which is in fact observed. According to our extension of Benedek's theory,[3,9] scattering from lakes in swollen corneas would result in straight lines of nonzero slope. Increasing values of the slope would represent a greater contribution from the lakes. This behavior is found in the measurements.

The transmission through several corneas was measured at each degree of swelling. Care must be exercised in analyzing the data to account properly for rabbit-to-rabbit variations in corneal thickness. For normal corneas, those variations alter F_T simply because of changes in Δ and do not reflect changes in the spatial distribution of collagen fibrils. In order to separate their effect, we average the quantity $(1/\Delta) \ln F_T$, which is equivalent to assuming that the variations in thickness result from variations in the amount of collagen laid down with an unvarying fibril distribution. In order to analyze the data from swollen corneas, we use the fact that the total number of fibrils remains constant; consequently,

$$\rho\Delta = \rho_0\Delta_0, \qquad (5)$$

where ρ_0 and Δ_0 are the initial (normal) fibril number density and thickness, respectively. Thus, the function that is averaged for the swollen corneas is

$$(\ln F_T/\Delta_0) = (\sigma_s \rho\Delta)/\Delta_0 = \sigma_s \rho_0. \qquad (6)$$

The experimental results are displayed in Fig. 4 for various degrees of swelling, R (swollen thickness/normal thickness). It must be stressed that the physiological conditions of the corneas were carefully monitored and controlled during the experiments. These precautions were of the utmost importance because light scattering is such a sensitive function of corneal thickness. In the figure, we have actually plotted the quantity $\lambda^3 \langle \rho_0 \sigma_s \rangle$, where the brackets denote the average value. The fact that the data from normal corneas are well fit by a straight line of zero slope supports the short-range ordering models

and dictates against the long-range ordering models, which predict a $1/\lambda^2$ dependence for this quantity. These data do not invalidate the equal refractive index model of transparency, but in the next section, we show that this model can be ruled out on the basis of the cornea's observed birefringence properties.

The data for the swollen corneas are fit by straight lines having positive slopes. This result dictates against the model relying on a homogeneous disruption of fibril positions. The data are consistent with the lake model. The value of the slope measures the lake contribution to the scattering, and, in agreement with electron micrographs, the data indicate that lakes are more important contributors at greater degrees of swelling. Also, the data suggest that lakes are present even at the lower degrees of swelling. Our electron micrographs show some evidence of lakes when the thickness ratios of the corneas are as small as 1.25 and definite evidence when the ratios are 1.5 or greater. In summary, the results of light scattering

experiments are consistent with the structural features shown in electron microscopy.

The fact that the light scattering measurements are consistent with the structures revealed in electron microscopy is encouraging, but one must remember that these comparisons assume that the collagen fibril matrix in the stroma is the primary source of scattering. Other investigators have questioned this assumption.[13] On the basis of their measurements of light scattering as a function of depth into the cornea, they concluded that the epithelial and endothelial cellular layers scattered more light than the stroma.[14] Such measurements are distorted by the finite resolution of the detection optics. By properly accounting for these distortions, we showed that their data actually suggest that most of the scattered light comes from the stroma. We also made similar measurements at a variety of scattering angles and showed that the same conclusion holds in all cases.[15] We are now making angular scattering measurements by which we hope to eliminate the possibility that the stromal scattering comes from its keratocyte population, thus further validating our underlying assumptions.

With respect to the theoretical analyses of light scattering, up to now it has only been possible to make quantitative calculations of the scattering from normal corneas. We are now developing methods based on the direct summation of scattered electric fields using the measured diameters and positions of the individual fibrils. These methods would be applicable to moderately swollen corneas and also to scarred corneas, whose fibrils have a wide range of diameters and whose spatial distributions are nonuniform, provided that they are sufficiently transparent for the Born approximation to hold. While they appear straightforward, the direct summation methods are complicated by an artifactual diffraction term. The term arises because the typical dimensions of the electron micrograph region from which the fibril positions are determined are only about 2 by 4 micrometers. The procedure then is to assume that this region is typical and extrapolate to the dimensions of the entire illuminated region (about 400 by 1000 micrometers). For corneas of normal thickness, the true scattering term is several orders of magnitude smaller than the diffraction term, and extreme care is required to extract it. We have made considerable progress on this problem and are confident that we have a tractable procedure, which we are testing by using it to calculate the scattering by normal corneas. In the future, we hope to tackle the problem of scattering from highly turbid corneas. We plan to develop variational methods based on the direct summation approach. Our experience with other random scattering problems indicates that those methods can account for interference, polarization, and multiple scattering.[16,17]

POLARIZED LIGHT SCATTERING

The methods described in the previous section all involve the scattering of unpolarized light; however, other useful structural information can be gleaned from the scattering of polarized light, especially at small angles. Indeed, polymer scientists have long used the small-angle light scattering (SALS) method as a standard tool for investigating polymer morphology.[18] It consists of illuminating the specimen with a collimated beam of plane polarized light from a laser and observing the light scattered at small angles. Two configurations are distinguished according to whether the collected scattered light is polarized the same as, or perpendicular to, the incident light. They produce characteristic light scattering patterns called, respectively, the $I_\parallel$ and $I_\perp$ patterns. The $I_\parallel$ pattern is caused by induced dipole oscillations that are parallel to the incident electric field vector. If the scatterers are either geometrically or optically anisotropic, or both, the induced dipole oscillations will also have a component perpendicular to the incident field. That component gives rise to the $I_\perp$ pattern.

Several other investigators had applied the SALS method to the cornea[19-22] and had interpreted their results in terms of structure models known from polymer physics. Unfortunately, the histological evidence for those models was less than satisfactory. Buoyed by our success with the direct approach of comparing measured scattering with predictions based on histological structures in the case of unpolarized light,[3,12] we decided to undertake our own investigation of corneal SALS. Our results, described below, show that the SALS patterns can be related to structures revealed by electron microscopy and that depolarized scattering can be used to obtain structural information about the architecture of the stromal layers.[23,24]

The SALS method probes structural features whose linear dimensions are on the order of several micrometers, significantly larger than those probed by the conventional techniques described in the previous section. The obvious micrometer-sized structures in the cornea are the cells within the epithelial, stromal, and endothelial layers and the thicknesses of the lamellae. We were also struck by the fact that low-power electron micrographs of the cornea always depicted the corneal lamellae as undulating, rather than smoothly following the overall corneal curvature (cf. Fig. 5). The undulations were usually dismissed as just another artifact of electron microscopy. We noted, however, that their average 14-micrometer period was consistent with the angular spread of existing corneal SALS patterns.[20] In discussions following the presentation of our unpolarized light scattering results at an international meeting, it was stated that the lamellae actually do appear flat in electron micrographs of corneas fixed with an applied pressure that simulates the normal intraocular pressure,[25] although no such micrographs had been published.

This observation, together with the fact that the earlier SALS work had been done on unpressurized corneas, provided the key to our initial SALS experiments. We suspected that the undulating lamellae might somehow act as a diffraction grating and
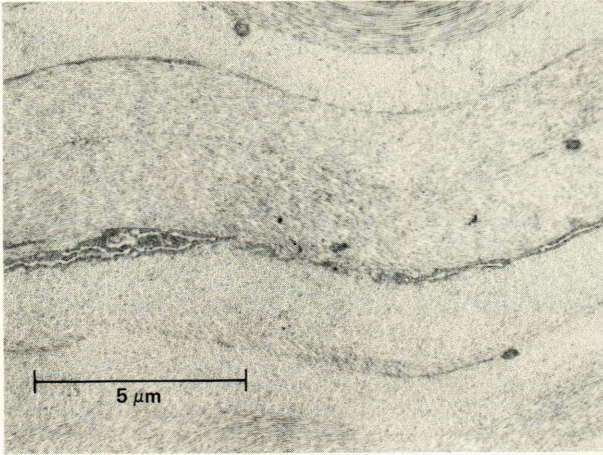
Figure 5 — Electron micrograph of the central portion of a rabbit cornea that was fixed without maintaining an applied pressure across the cornea. Several lamellae are shown, and they undulate with a period of about 14 micrometers.

thereby produce the four-lobed cloverleaf pattern that others had observed with rabbit corneas.[20] In those patterns, the intensity maxima at a scattering angle of about 2° were consistent with a 14-micrometer spacing in a Bragg-like diffraction condition. With this as our working hypothesis, we set out to discover the influence of physiological conditions, particularly intraocular pressure, on the cornea's SALS properties. At the same time, we began to devise a method for preparing corneas for electron microscopy that maintained an applied pressure. We also began to develop theoretical techniques for calculating the SALS patterns from wavy corneal lamellae.

The SALS apparatus is shown in Fig. 6.[23,24] The polarization rotator selects the polarization direction of the incident light, and the aperture blocks stray polarized light from falling on the cornea. Provisions for applying a hydrostatic pressure behind the cornea are included. The rotating analyzer is used to select either the $I_\perp$ or the $I_\parallel$ mode. Figure 7 shows the $I_\perp$ scattering patterns from an excised cornea at three

pressure levels.[24] The zero pressure pattern is similar to that observed by the earlier investigators. The new finding is that the pattern disappears at the rabbit's normal intraocular pressure of 18 mmHg, which is consistent with our hypothesis that the undulating lamellae cause the SALS pattern. We also found similar results with corneas that had both their endothelial and epithelial cell layers removed, thus eliminating those structures as possible sources of the observed SALS. In addition, we later obtained similar results with bovine corneas. Subsequently, we confirmed that the lamellae indeed straightened in electron micrographs (cf. Fig. 8) of corneas fixed with an applied transcorneal pressure. On the basis of this evidence, we concluded that our working hypothesis was correct.[24]

The results of these experiments not only satisfied our objective of explaining the histological basis of corneal SALS, but also showed that the wavy lamellae are a property of unpressurized tissue and are not introduced by the fixative *per se*. While performing these experiments, we made several other noteworthy observations. Like others,[19-22] we noted that transmission through the analyzer in the $I_\perp$ configuration varies substantially, depending on the direction of the incident polarization, and that the sharpest SALS patterns (like those in Fig. 7) are obtained at the setting that minimizes this $I_\perp$ transmission. Away from this setting, the patterns become less distinct. We also noticed that, no matter what the setting, the lobes of the $I_\perp$ pattern always align with the polarizer and analyzer axes directions. The remainder of this section deals with the development of our SALS theory and shows how the interplay between theory and experiments enabled us to extract significant information from these and other experimental observations.

Since no theory existed, we had to devise one to predict the light scattering from an assembly of long, thin, wavy, dielectric cylinders such as the wavy collagen fibrils shown in the electron micrographs of unpressurized corneas. The theory was developed in collaboration with R. H. Andreo (formerly of the APL Milton S. Eisenhower Research Center); his contributions were essential. The first step was to cal-
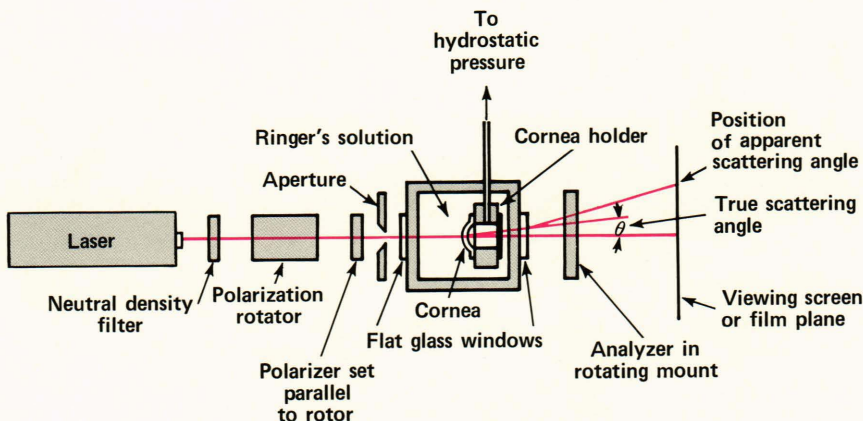

Figure 6 — A schematic diagram of the apparatus for recording SALS patterns from the cornea. The polarization direction of the incident radiation can be varied by means of the polarization rotator. As with our unpolarized light scattering measurements, we have made provision for applying a transcorneal pressure during the measurement.
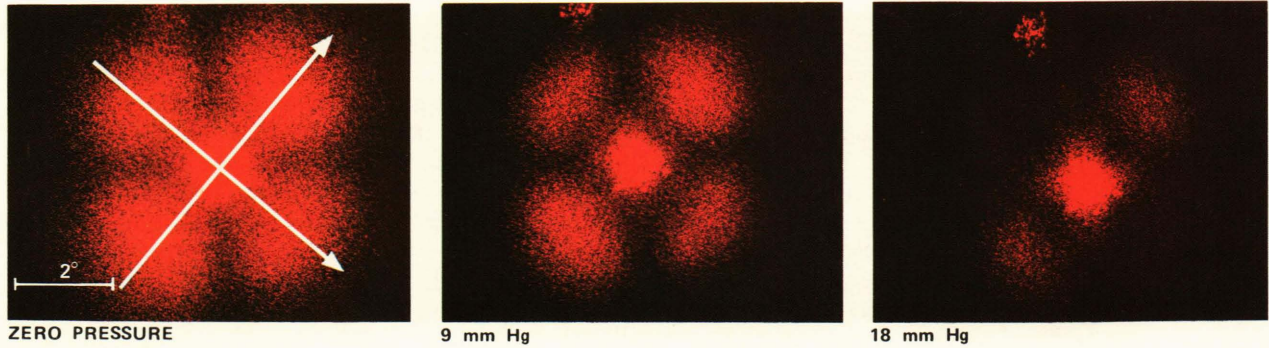
ZERO PRESSURE   9 mm Hg   18 mm Hg

Figure 7 — The effect of increasing transcorneal pressure on the $I_\perp$ scattering from rabbit cornea. The outer lobes define the axes shown by the arrows. Experimentally, we find that these axes are aligned with the crossed polarizer and analyzer directions. For the figure, the crossed polarizer directions are aligned to minimize the transmitted power. The scale for the true scattering angle is given on the first plate. All plates were exposed and processed identically.
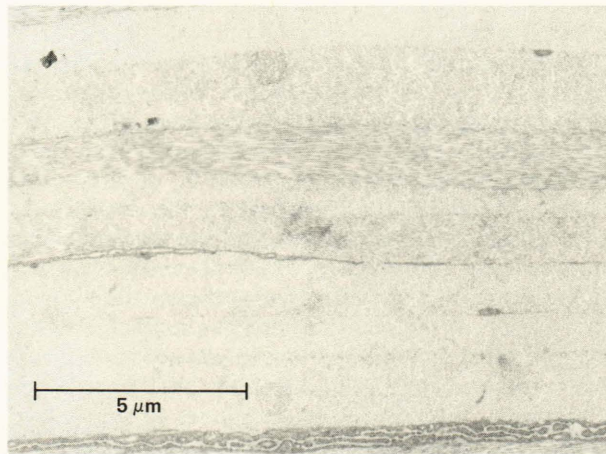

Figure 8 — Electron micrograph of the central portion of a rabbit cornea that was fixed with an applied pressure difference of 18 mmHg to simulate the normal intraocular pressure. This cornea was from the mate of the eye used for Fig. 5. Note that the lamellae are essentially straight.

culate the scattering from an isolated wavy fibril. In the Born approximation, this scattering intensity has the form of a series of diffraction lines and, unfortunately, is dominated by the lowest order line whose intensity is independent of scattering angle (at small angles). From this, we showed that an assembly of such fibrils, acting as independent scatterers and having an arbitrary distribution of orientation angles, could not produce the scattering-angle dependence of the experimental patterns.[26]

This disagreement should not be too surprising because the fibrils are not independent scatterers. Indeed, as discussed in the preceding section, corneal transparency depends critically on the correlations in the spatial positions of fibrils. Moreover, and more important, the orientation and waviness of the fibrils in a given lamella are not arbitrary; rather, the fibrils are parallel to one another and undulate in phase. We demonstrated that the effect of these correlations is to produce scattering that is characteristic of a wavy sheet.[26] We showed that the electric susceptibility

tensor of the effective homogeneous wavy sheet can be expressed directly in terms of the individual fibril susceptibility, thereby relating a macroscopic property of the sheet to the corresponding microscopic property of its constituent fibrils.

The Born approximation theory predicts that the scattering from a single undulating lamella is a series of bright spots located at an azimuthal direction along the mean fibril axis and at scattering angles, θ_m, that obey a diffraction condition

$$m\lambda = \Lambda \sin \theta_m. \tag{7}$$

Here, m is the diffraction order, λ is the wavelength of the light in the cornea, and Λ is the spatial period of the undulations. The intensity of these spots falls off rapidly with increasing order. Choosing $\Lambda = 14$ micrometers, in agreement with corneal electron micrographs, yields $\theta_1 = 2°$, which is in excellent agreement with the scattering angle at which the experimental patterns[20,23,24] exhibit their peak intensities.

The scattering pattern to be expected from a cornea is obtained by integrating the single-lamella results over the distribution of lamellar orientations. Because the single-lamella diffraction spots are restricted to an azimuthal direction along the mean fibril axis, scattering in a particular azimuthal direction comes entirely from lamellae oriented in that direction. Thus, if the distribution of orientations were uniform, the intensity of the SALS pattern would vary with azimuthal angle in the same way that the intensity of the diffraction spot varies with ζ, the angle the mean fibril axis makes with the polarization vector of the incident field. The fibril's geometric and polarizability axes are in the same direction for isotropic fibrils, and the spot intensity would vary as $\sin^2(2\zeta)$, whereas it would vary as $\cos^2(2\zeta)$ for strongly anisotropic fibrils because their geometric and polarizability axes are at 45° to each other. Thus, the predicted pattern would have four maxima as a function of azimuthal angle and, only for anistropic fiberils would these maxima be aligned with analyzer and polarizer directions as observed experimentally. Although these conclusions are based on a uniform

72

orientation model, we will show that, for the conditions of the SALS experiments of Fig. 7, similar results hold for the more general orientation distribution models suggested by other light scattering measurements related to the cornea's birefringent properties and by electron microscopy.

As noted earlier, the fact that the lobe-analyzer alignment is maintained with tandem rotations of the analyzer and polarizer in the crossed configuration shows that there must be some fibrils (lamellae) pointing in every azimuthal direction. However, other observations rule out a completely uniform lamellar orientation model. In particular, because there are no preferred azimuthal directions in a uniform lamellar orientation model, it is inconsistent with the fact that the crossed polarizer pattern varies with such tandem rotations and that the $I_\perp$ transmission also varies with those rotations. The variable transmission in this crossed polarizer configuration is a manifestation of the cornea's birefringence, which produces different amounts of depolarization, depending on the polarization direction of the incident beam.

Figure 9 illustrates how this transmission varies with polarizer orientation. The minimum transmission value is approximately two orders of magnitude greater than the "leakage" through the apparatus when the specimen is removed. This indicates that the emerging light is elliptically polarized, which is another characteristic of birefringent material. Such birefringence implies the existence of oriented structures in the sample. Indeed, the observed dependence on polarizer orientation is consistent with distributions that have either one or two preferred directions superimposed on a uniform distribution, as is also suggested by electron microscopy.[24] But the transmission data show that if there are two preferred directions of lamellar orientation, then they must be orthogonal; otherwise, the maxima and minima would not alternate at 45° intervals. Moreover, if the distribution has two preferred directions at right angles, then there cannot be equal numbers of fibrils pointing in each of them, for if there were, a straightforward analysis[27] shows that the transmission would be angle-invariant because the orthogonal fibrils would cancel each other's effect in pairs.

By measuring the total power in the incident beam, we also showed that 40% of the transmitted field is depolarized at the setting that produces the maximum $I_\perp$ transmission. This observation bears on the transparency theories discussed in the first section. In particular, this large amount of depolarization means that there is substantial scattering. Thus, the equal refractive index explanation of transparency[8] is untenable, and transparency results from interference among the waves scattered by the different fibrils.

In general, the existence of either one or two preferred orientation directions in the models suggested by the data in Fig. 9 would affect the predicted SALS patterns. The patterns in Fig. 7, however, were obtained at the condition of minimum $I_\perp$ transmission,
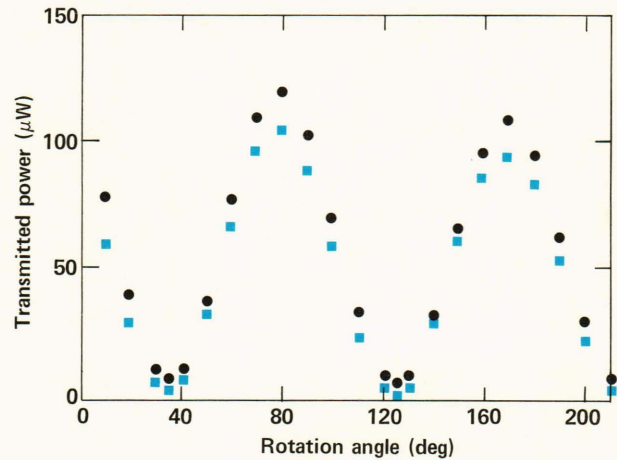

Figure 9 — Power transmitted through the rabbit cornea of Fig. 7 in the $I_\perp$ configuration as the polarization direction of the incident light and the crossed analyzer are rotated in tandem. The circles are at zero pressure, and the squares are at 18 mmHg pressure. The periodic variation with rotation angle shows that the distribution of lamellar orientations is not uniform; rather, there is either one preferred orientation direction or two that are at right angles to one another.

i.e., at the condition of minimum depolarization. It is straightforward to show that this condition would occur when the fibrils pointing in the preferred directions do not produce any depolarization, i.e., when the polarizer is at 45° to one of the preferred directions. Thus, the $I_\perp$ SALS pattern in this setting is produced entirely by the remaining lamellae that are not in the preferred directions. This justifies our claim that, at this setting, averaging over lamellar orientations in these models is the same as averaging over a uniform distribution of orientations. Therefore, the theory predicts a four-lobed pattern in agreement with experiments.[26]

It is also interesting that, in the setting that produces the minimum transmission, the analyzer has a specific orientation relative to the overall corneal geometry. Thus, the preferred lamellar directions are the same for each animal of a particular species.

Although we were pleased with this success of the theory, we were initially puzzled by the fact that the features of the experimental SALS pattern were blurred at the setting for maximum $I_\perp$ transmission. Indeed, our theory predicts that the sharpest patterns should occur at the maximum $I_\perp$ transmission. There, the analyzer and polarizer are aligned so that the fibrils in the preferred directions produce the peak intensities in the lobes, which, therefore, should be brighter. The resolution of this apparent conflict between the theory and experiments resides in the large depolarization of the incident beam indicated by Fig. 9. In particular, our theory is based on the Born approximation, which approximates the field incident on any fibril in the cornea by the incoming linearly polarized plane wave. The approximation assumes, therefore, that neither the irradiance nor the polarization of the beam is affected significantly dur-

ing its passage through the cornea. Standard transmission measurements, such as those in the previous section, show that the irradiance of the transmitted beam is virtually unchanged. However, as noted above, 40% of the incident field emerges depolarized at the maximum $I_\perp$ transmission setting, while less than 10% is depolarized at the setting for minimum $I_\perp$ transmission.

Thus, our theory should hold at the minimum setting but not at the maximum. Although we have not made detailed calculations based on improvements in the Born approximation, we have developed a heuristic explanation of the washed-out appearance of the SALS pattern. The small-angle $I_\parallel$ scattering pattern from incident light polarized parallel to the analyzer direction is also a four-lobed cloverleaf, but it is rotated 45° relative to the $I_\perp$ pattern.[23,24,26] At the maximum $I_\perp$ transmission setting, there is a large depolarized field incident on the back layers of the cornea that therefore produces an appreciable $I_\parallel$ pattern superimposed on the $I_\perp$ pattern. This superimposed $I_\parallel$ pattern fills in the spaces between the lobes of the $I_\perp$ pattern and blurs its appearance.

Several interesting problems remain to be solved. For example, a better understanding of plane wave propagation through layered anisotropic media is needed to make quantitative improvements in the Born approximation. In addition, we must develop more realistic structure models of the stromal lamellae. Electron microscopy shows that fibril axes in adjacent lamellae make large angles with one another and that the lamellae pack without gaps in the unpressured state (cf. Fig. 5). The rigid corrugations assumed in our present model would not permit such stacking without the formation of gaps, and so more general waveforms are required. The appropriate forms are being investigated experimentally, and theoretical methods of calculating the scattering are being developed. If history repeats, we expect these endeavors to yield further structural insights and to provoke further interesting research questions.

STRUCTURAL ALTERATIONS FROM INFRARED RADIATION

Although transparency demands that the cornea not significantly absorb visible light, it does absorb in the ultraviolet and infrared parts of the electromagnetic spectrum. In the infrared, the absorbed radiation can cause damage by raising the temperature of the tissue. Because of the widespread use of CO_2 lasers, corneal damage resulting from exposure to the 10.6-micrometer radiation they emit is well documented.[28-31] The absorption length of CO_2 laser radiation in water is only about 10 micrometers. Thus, the radiation is absorbed entirely within the water of the epithelial cells. Consequently, epithelial damage received most of the attention of the early investigators in this field. Minimal epithelial damage is characterized by a relatively faint, gray-white area that is visible with the slit lamp 30 minutes after exposure.[32] The early workers determined threshold exposure levels, that is, the combinations of beam irradiance and exposure time that produce this type of damage.

Heat conduction causes some of the thermal insult from those exposures to spread to the endothelium, and some evidence of altered endothelial integrity following exposures at or slightly above the epithelial damage threshold has been reported.[33] In addition, there are ever-increasing industrial and military uses of other lasers that operate at shorter infrared wavelengths (e.g., holmium at 2.06 micrometers and erbium at 1.54 micrometers). Radiation at those wavelengths would also be strongly absorbed by the water of the cornea although not nearly as strongly as 10.6-micrometer radiation. The absorption length in water at the shorter wavelengths is comparable to and even larger than the thickness of the cornea, so this radiation would penetrate the cornea and cause a more uniform temperature increase throughout its depth.

In general, one would expect this more uniform heating to produce endothelial damage at or even below the epithelial damage threshold, especially if the endothelium were more sensitive than the epithelium to temperature increases. The consequences of endothelial damage can be more serious than epithelial damage, which appears to heal quickly. The endothelium plays a vital role in maintaining corneal thickness. In the human, it appears to repair itself by a mechanism in which the remaining cells slide and enlarge to fill in the gaps left by lost cells.[34] Thus, repeated exposures in an unprotected environment could lead to permanent corneal clouding because of the impaired ability to maintain normal corneal thickness.

Because of the serious nature of this potential health hazard, we initiated a multidisciplinary approach to corneal infrared damage in collaboration with Col. Edwin Beatrice and Mr. Bruce Stuck of the Letterman Army Institute of Research. Our approach involves theoretical calculations of the temperature/time histories caused by the exposure, measurements of temperature increases resulting from exposure to the beam from a CO_2 laser, and histological documentation of structural alterations caused by exposure levels near the damage threshold. The calculated temperatures allow us to interpret our damage thresholds in terms of the thermal history of the tissue. The calculations were verified experimentally using a CO_2 laser, and we have used that laser for our damage threshold determinations. We use the CO_2 laser in this research in order to take advantage of the ease with which its mode quality, irradiance level, and exposure duration can be controlled. These characteristics are highly variable in other infrared lasers. Moreover, the use of thermal models allows results obtained with the CO_2 laser to be extended to other wavelengths by appropriate calculations, which are possible because the absorption coefficient of the cornea is known throughout the infrared, and its thermal properties closely approximate those of wa-

ter. For the experiments, the laser is operated in the
TEM_{00} mode because its Gaussian irradiance profile
is reproducible and lends itself to easy analysis.

In the remainder of this section, we will describe
the research that has led us to conclude that all cor-
neal cells – epithelial, endothelial, and stromal –
have similar thermal damage mechanisms. For single
exposures having durations between approximately
1/20 and 1 second, cellular damage is associated with
the cells achieving a sharply defined peak tempera-
ture. Other single-pulse experiments at both shorter
and longer exposure durations, as well as experi-
ments involving exposures to sequences of subthresh-
old pulses, have shown deviations from this simple
"critical temperature" damage model. The implica-
tions of these experiments with regard to other possi-
ble damage models are discussed.

In order to gain a better understanding of endothe-
lial damage caused by exposure to infrared radiation,
it is important to know the endothelial temperature/
time history. We have elected to calculate the histo-
ries for a range of laser parameters and to verify the
calculations and underlying assumptions with a CO_2
laser. The Green function solution to the heat flow
equation for a Gaussian beam incident on a semi-in-
finite slab has been discussed by Chang and
Dedrick,[35] who expressed the temperature at any lo-
cation within the eye as a definite integral. We have
evaluated that integral numerically to obtain the time
course of temperature at several points on the endo-
thelium for various exposures. Typical results for
10.6-micrometer radiation are illustrated by the
curves in Figs. 10a and 10b. The calculations assume
that there is no heat transfer from the epithelium
back into the air, that there is a good thermal contact
with the bathing medium at the endothelial side, and
that the thermal conductivity and the absorption co-
efficient (in the exponential Beer-Lambert absorp-
tion law) of the cornea can be approximated by their
values for water. Also shown in the figure are experi-
mental values for the endothelial temperature in-
crease measured with a very fine gauge thermocouple
placed at the endothelium on the beam axis.[36] The
agreement is sufficiently close to show the validity of
the calculations and their underlying assumptions. In
other experiments using a liquid crystal technique,
the off-axis temperature predictions were verified as
a further check on the validity of the calculations.

In Fig. 10a, the exposure time (0.104 second) is ap-
proximately that of an epithelial damage threshold
exposure for 24 watts per square centimeter peak ir-
radiance.[31-33] In the histological experiments dis-
cussed below, we found that the 5 to 6°C increase in
endothelial temperature caused by such exposures is
insufficient to produce damage. The longer 1.04-sec-
ond exposure in Fig. 10b resulted in a temperature
rise of 45°C. That exposure corresponds to one of
the endothelial damage thresholds that we found in
our damage experiments.[37]

We use a wet staining technique to determine endo-
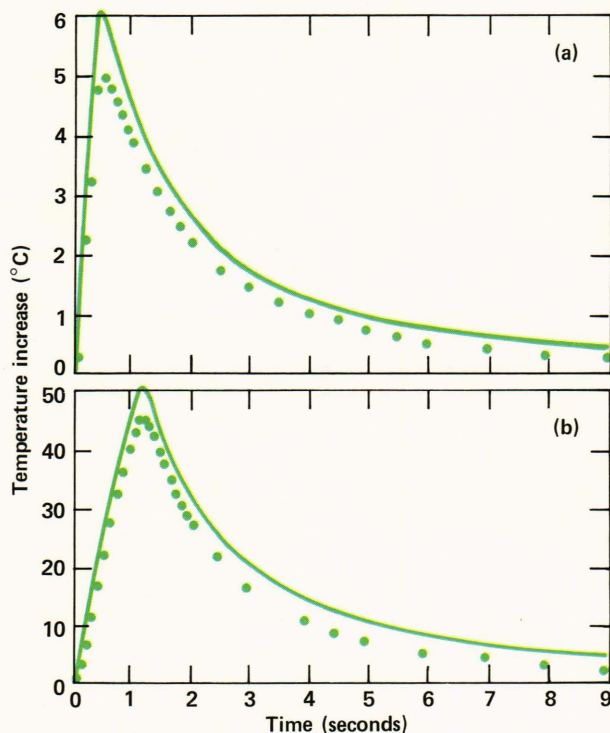thelial damage thresholds and to characterize the re-

Figure 10 — The temperature histories on the beam axis at
the endothelium of a cornea exposed to 24 watts per square
centimeter. The cornea thickness was 0.38 millimeter. The
dots correspond to the temperatures measured with a 25-
micrometer thermocouple positioned on the beam axis at
the endothelial surface. The lines are the calculated tem-
peratures for the same position. In (a), the exposure time
was 0.104 second, which corresponds to the threshold for
epithelial damage at this irradiance. In (b), the exposure
time was 1.04 seconds, which corresponds to the threshold
for endothelial damage.

sultant lesions. The stains are alizarin red S to outline
the cell borders and either trypan blue or indocyanine
green to penetrate and thereby identify damaged
cells.[37] Figure 11 illustrates threshold endothelial
damage produced by exposure to a beam having a
peak irradiance of 10 watts per square centimeter for
5.24 seconds. The distorted cells and uneven staining
of the cell borders are characteristic of threshold le-
sions. In particular, much of each damaged cell bor-
der is more heavily stained than are normal cell bor-
ders, yet other parts of the damaged cell borders are
often completely unstained. Another common fea-
ture of these lesions is that the boundary between the
damaged area and the adjacent apparently normal
cells is sharply delineated. The pulse durations that
produce threshold damage are clearly defined; endo-
thelia of corneas irradiated for 90% of the threshold
duration are indistinguishable from those of nonir-
radiated corneas. The exposure conditions in Figs.
10b and 11 (which cause minimal endothelial dam-
age) produce a 45°C temperature rise at the endothe-
lium.[37] In both of these cases, the exposure durations
were ten times those required to produce minimal ep-
ithelial damage at the respective irradiance levels.
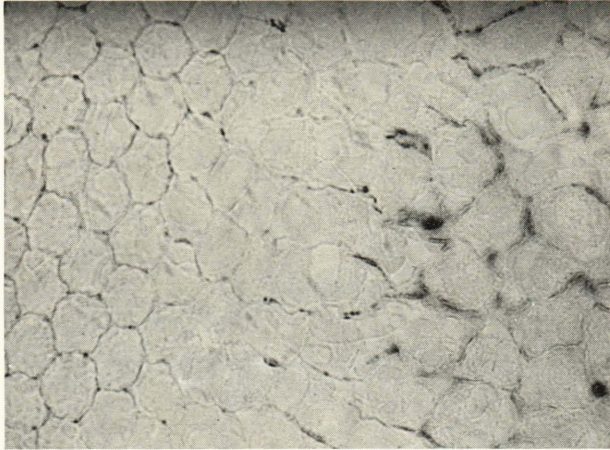Thus, with a CO_2 laser, protecting against epithelial

Figure 11 — A photograph of the border area of a threshold endothelial lesion. The exposure was 10 watts per square centimeter for 5.24 seconds. The endothelium has been stained with alizarin red and indocyanine green. The nearly hexagonal cells at the left are essentially normal. There is a sharp delineation between these and the damaged cells. In this case, the dark indocyanine green-stained cells are associated with a folding artifact.

damage will certainly ensure endothelial integrity. However, our calculations indicate that for other, more penetrating infrared wavelengths, the temperature rise throughout the cornea can be nearly uniform. Thus, for these wavelengths, the damage-threshold exposures of endothelium and epithelium would be essentially the same because, as discussed below, epithelial-damage-threshold exposures increase the temperature of the epithelium by 45°C.[32]

During the investigation of endothelial damage, we noted that corneas exposed to greater than the epithelial damage threshold, but to less than the endothelial damage threshold, develop a bowl-shaped region in the stroma that is devoid of cells 48 hours after exposure.[38] At that time, such corneas have recovered their normal thickness and have regrown a smooth epithelium. Figure 12, a composite of several light micrographs, clearly shows this acellular region. The border between the acellular region and the region containing undamaged keratocytes is sharply delineated. The abruptness of the demarcation suggests that keratocyte damage is also a sensitive function of the temperature history. We used high-magnification
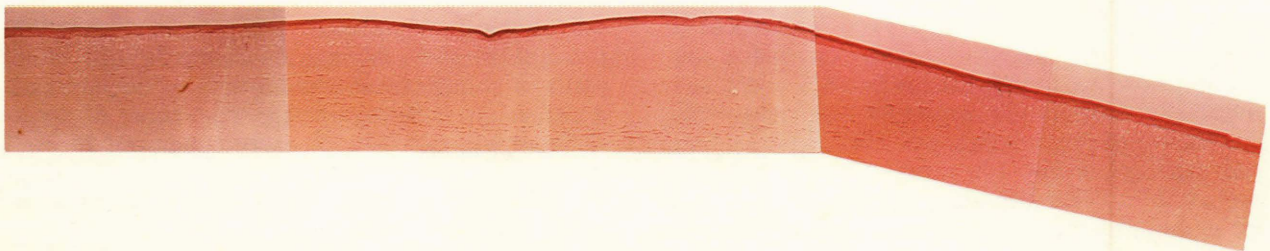
slit lamp photographs taken just before sacrificing the animal for histology to measure the profile of the lesion. Figure 13 shows the lesion border positions determined in this manner for a cornea exposed to a peak irradiance of 9.7 watts per square centimeter for 2.5 seconds. The lines in the figure are calculated maximum-temperature-increase isotherms. These results suggest that a temperature increase of 45 to 50°C is needed to damage a keratocyte.[38] This increase is similar to the one we found for minimal endothelial cell damage and to the increase that produces minimal epithelial damage.[31-33,37,38]

The infrared damage discussed up to now has been from single-pulse exposures. However, range finders, target designators, communication devices, and other infrared instruments used by the military emit sequences of pulses. Prior to our work, there were no data on corneal damage from exposure to multiple subthreshold pulses. Pulse trains are characterized by the irradiance along the beam axis, I_0; the beam diameter, d; the total number of pulses in the train, N; the pulse repetition frequency, PRF; and the duration of the individual pulses, τ. In our initial experimental protocol, the parameters I_0, d, N, and PRF were fixed and τ was varied in order to determine the minimum pulse width that produced epithelial damage. The procedure was repeated as N, PRF, and I_0 were varied systematically. We use the usual criterion for minimal epithelial damage, i.e., the development of a faint gray-white area, to determine the damage threshold.[32]

Figure 14 shows the calculated temperature histories on the beam axis at a depth of 10 micrometers in the cornea (a depth chosen to be just into the epithelium, assuming that the thickness of the tears that cover the epithelium is about 5 to 7 micrometers). The calculations are for various threshold values of τ and N when $I_0 = 10$ watts per square centimeter. In each case, the maximum temperature increase is about 45°C, and this same temperature increase also is found for the threshold exposures at a peak irradiance of 46 watts per square centimeter. These results are consistent with a critical temperature damage model.

Other researchers had postulated a damage integral model to correlate epithelial thresholds for single-pulse exposures. In this model, an Arrhenius-like
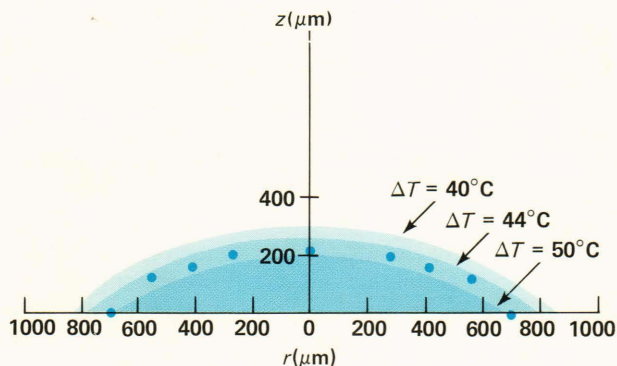

Figure 12 — A montage of light micrographs of a stromal lesion 48 hours after an exposure of 26 watts per square centimeter for 0.4 second. The essentially acellular lesion extends about halfway through the stroma. The lesion is bordered by normal (but perhaps slightly swollen) keratocytes.

Figure 13 — Measured position of the border of a bowl-shaped stromal lesion. The points are measured from a highly magnified slit lamp photograph taken 48 hours after an exposure of 9.7 watts per square centimeter for 2.5 seconds. The curves are calculated isotherms of peak temperature increase.

factor $\exp[-E/kT(t)]$ is introduced, in which k is the Boltzmann constant, $T(t)$ is the temperature history (in K) for the experimentally determined threshold exposure, and E is an effective energy parameter. This model postulates that damage will occur when the time integral of the Arrhenius factor exceeds a certain value. The marked differences in the time courses of the temperatures in the multiple-pulse threshold exposures in Fig. 14 are inconsistent with this type of damage integral model.

Discussions with our colleagues at the Letterman Army Institute of Research led us to modify our experimental protocol to keep the pulse width constant (at 10 milliseconds) and to determine the peak irradiance that causes threshold epithelial damage for different numbers of pulses. The temperature calculations for these experimental damage thresholds showed some deviations from the fixed critical temperature for damage that we had found consistently in earlier experiments. In some cases, the calculated peak temperature increase at threshold is as high as 68°C. In order to understand better the source of these deviations from an essentially fixed critical temperature increase of 45°C, we decided to reinvestigate the single-pulse epithelial damage thresholds. The existing threshold data determined for short (less than 30 milliseconds) and long (greater than 500 milliseconds) single-pulse epithelial exposures were scarce and somewhat unreliable.[32] Our single-pulse experimental findings are summarized in Table 1. They show that while a simple critical-temperature model correlates the damage very well for exposure durations between 30 and 500 milliseconds, significant deviations occur at both shorter and longer exposures.

For exposures of 30 milliseconds and longer, the temperature thresholds fit an empirical equation of the form $T_c = 75.5 t^{-0.026}$ (°C), where the exposure time, t, is in seconds. This relation is close to the one Egbert and Maher[32] used to correlate quite scattered data from a number of sources.
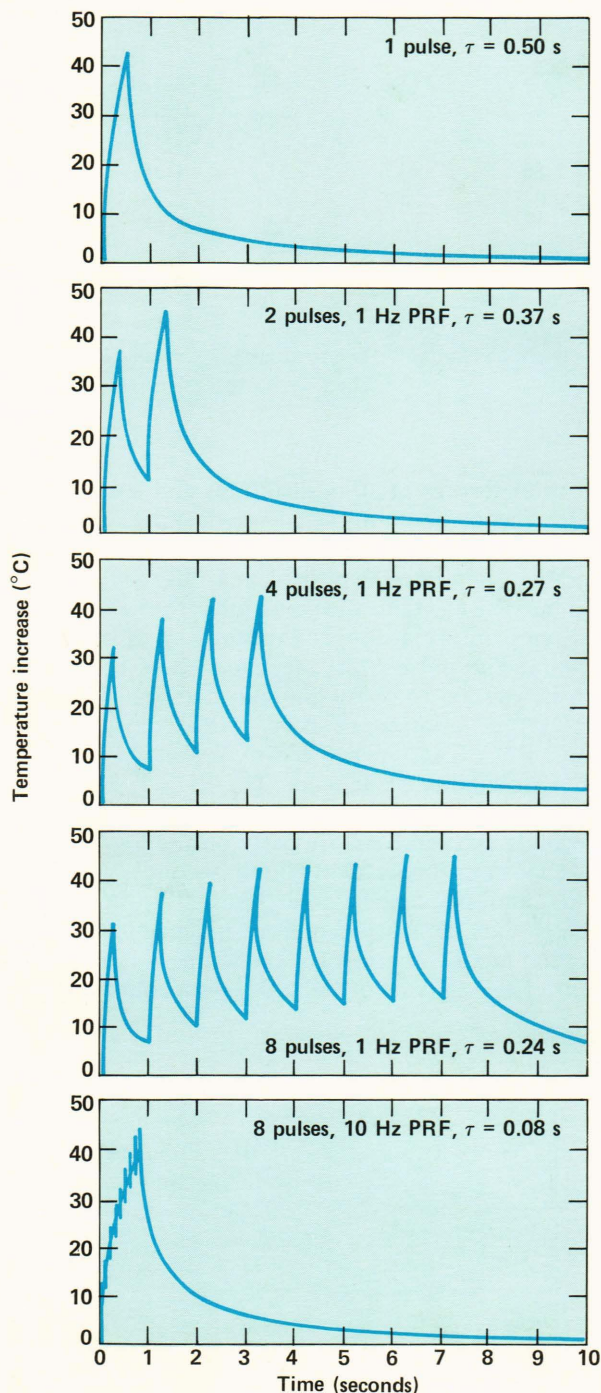

Figure 14 — Calculated temperature histories for epithelial threshold damage from multiple pulse exposures. The temperatures are calculated at a point on the incident beam axis 10 micrometers into the cornea. Note that, despite the wide variability of the temperature histories, epithelial damage in each case is associated with a temperature increase of about 45°C. (Beam diameter is 2.17 millimeters; irradiance is 10 watts per square centimeter.)

Table 1 – Epithelial damage thresholds for single-pulse exposures.

1/e Diameter of Gaussian Beam (mm)	Peak Irradiance (W/cm²)	Pulse Width (ms)	ED₅₀ (J/cm)²	ΔT_max * (°C)
2.34	148.8	9.6	1.43	73.6
2.44	88.8	17.9	1.59	65.2
2.40	60.8	23.7	1.44	52.9
1.86	44.6	31	1.38	45.4 †
2.0	24.5	100	2.45	47.8
2.16	10.0	500	5.00	43.5
2.44	6.52	977	6.37	38.7
2.44	3.02	9730	29.4	36.0

*Calculated at a depth of 10 micrometers.

†Exposure conditions for which a critical temperature damage model holds.

For exposures of 30 milliseconds and less, there is an interesting break in the curve when peak temperature data are plotted against exposure time. In order to gain insight into the possible reasons for this break and into the origin of the deviations from a fixed critical temperature at longer exposures, it is helpful to examine the pulse width dependence of the energy density needed to cause minimal damage. Figure 15 shows the variation of ED_{50} with exposure time, where ED_{50} is the energy density for which there is a 50% probability of damage. The ED_{50} is essentially constant for exposure durations below about 50 milliseconds and increases (linearly on the log-log plot) for exposures longer than 50 milliseconds. The ED_{50} values and their associated exposure times are experimental data and are therefore independent of the thermal model assumed for the temperature calculations. The behavior of the ED_{50} data could possibly

be explained by assuming a different damage mechanism for exposures shorter than 50 milliseconds. They could also possibly be explained by postulating that a thermally isolated epithelium would sustain damage when it absorbed a certain amount of energy. That energy might, for example, be used to raise the temperature of the cells and to supply the latent heat needed to cause an endothermic phase change (such as protein denaturation, alterations of the organization of the lipids in the cell membranes, etc.). In the intact nonthermally isolated epithelium, however, some of the energy would flow out because of thermal conduction into the stroma and evaporation at the anterior surface. Thus, the qualitative features of Fig. 15 could be explained if the time constant of the loss processes were ≥ 50 milliseconds. We intend to explore the possibility that including evaporation and other phase changes in the temperature calculations will lead to a consistent thermal damage model.
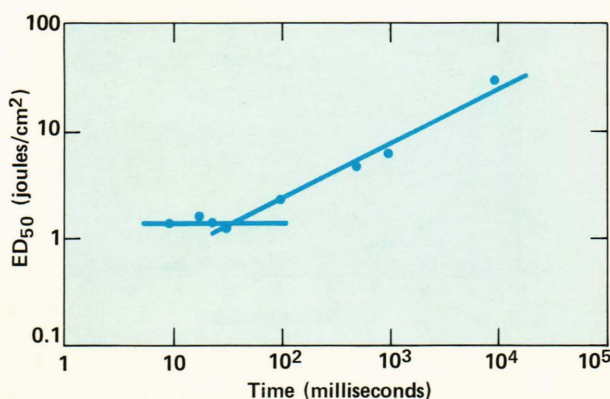

Figure 15 — The energy density for which there is a 50% probability of epithelial damage from single-pulse exposures as a function of exposure duration. Note that ED_{50} is constant for exposures shorter than 50 milliseconds. ED_{50} is a measured quantity and, unlike the temperature calculations, is independent of any assumed thermal model.

REFERENCES

[1] D. M. Maurice, "The Structure and Transparency of the Cornea," *J. Physiol.* **136**, 263-286 (1957).

[2] J. L. Cox, R. A. Farrell, R. W. Hart, and M. E. Langham, "The Transparency of the Mammalian Cornea," *J. Physiol.* **210**, 601-616 (1970).

[3] R. A. Farrell, R. L. McCally, and P. E. R. Tatham, "Wavelength Dependencies of Light Scattering in Normal and Cold Swollen Rabbit Corneas and Their Structural Implications," *J. Physiol.* **233**, 589-615 (1973).

[4] R. W. Hart and R. A. Farrell, "Light Scattering in the Cornea," *J. Opt. Soc. Am.* **59**, 766-774 (1969).

[5] R. A. Farrell and R. W. Hart, "On the Theory of the Spatial Organization of Macromolecules in Connective Tissue," *Bull. Math. Biophys.* **31**, 727-760 (1969).

[6] R. W. Hart, R. A. Farrell, and M. E. Langham, "Theory of Corneal Structure," *APL Tech. Dig.* **8**, 2-11 (1969).

[7] T. Feuk, "The Wavelength Dependence of Scattered Light Intensity in Rabbit Corneas," *IEEE Trans. Biomed. Eng.* **BME-18**, 92-96 (1971).

[8] J. W. Smith and J. Frame, "Observations on the Collagen and Protein-polysaccharide Complex of Rabbit Corneal Stroma," *J. Cell Sci.* **4**, 421-436 (1968).

[9] G. B. Benedek, "Theory of Transparency of the Eye," *Appl. Opt.* **10**, 459-473 (1971).

[10] V. Twersky, "Transparency of Pair-Correlated, Random Distributions of Small Scatterers with Applications to the Cornea," *J. Opt. Soc. Am.* **65**, 524-530 (1975).

[11] J. N. Goldman, G. B. Benedek, C. H. Dohlman, and B. Kravitt, "Structural Alterations Affecting Transparency in Swollen Human Corneas," *Invest. Ophthalmol.* **7**, 501-519 (1968).

[12] R. A. Farrell and R. L. McCally, "On Corneal Transparency and Its Loss with Swelling," *J. Opt. Soc. Am.* **66**, 342-345 (1977).

[13] J. I. Lindstrom, T. Feuk, and B. Tengroth, "The Distribution of Light Scattering from the Rabbits' Cornea," *Acta Ophthalmol.* **51**, 656-669 (1973).

[14] R. A. Farrell and R. L. McCally, "On the Interpretation of Depth Dependent Light Scattering Measurements in Normal Rabbit Corneas," *Acta Ophthalmol.* **54**, 261-270 (1976).

[15] R. L. McCally and R. A. Farrell, "Measurements of the Depth Dependence of Light Scattering in the Cornea," *Exp. Eye Res.* **23**, 69-81 (1976).

[16] J. A. Krill and R. A. Farrell, "Comparisons between Variational, Perturbational, and Exact Solutions for Scattering from a Random Rough Surface Model," *J. Opt. Soc. Am.* **68**, 768-774 (1978).

[17] J. A. Krill, R. H. Andreo, and R. A. Farrell, "Variational Calculations of Electromagnetic Scattering from Two Randomly Separated Rayleigh Dielectric Cylinders," *J. Opt. Soc. Am.* **73**, 408-410 (1983).

[18] J. C. W. Chien, "Solid State Characterization of the Structure and Property of Collagen," *J. Macromol. Sci. Rev. Macromol. Chem.* **C-12**, 1-80 (1975).

[19] F. A. Bettelheim and D. Kaplan, "Small Angle Light Scattering of Bovine Cornea as Affected by Birefringence," *Biochim. Biophys. Acta* **313**, 268-276 (1973).

[20] E. P. Chang, D. A. Keedy, and J. C. W. Chien, "Ultrastructures of Rabbit Corneal Stroma: Mapping of Optical and Morphological Anisotropies," *Biochim. Biophys. Acta* **343**, 615-626 (1974).

[21] F. A. Bettelheim and M. Kumbar, "An Interpretation of Small-Angle Light Scattering Patterns of Human Cornea," *Invest. Ophthalmol.* **16**, 233-236 (1977).

[22] F. A. Bettelheim and R. Magrill, "Small Angle Light Scattering Patterns of Corneas of Different Species," *Invest. Ophthalmol.* **16**, 236-240 (1977).

[23] R. L. McCally and R. A. Farrell, "Effect of Transcorneal Pressure on Small Angle Light Scattering from Rabbit Cornea," *Polymer* **18**, 444-448 (1977).

[24] R. L. McCally and R. A. Farrell, "Structural Implications of Small-Angle Light Scattering from Cornea," *Exp. Eye Res.* **34**, 99-113 (1982).

[25] J. Francois (private communication).

[26] R. H. Andreo and R. A. Farrell, "Corneal Small-Angle Light Scattering Patterns: Wavy Fibril Models," *J. Opt. Soc. Am.* **72**, 1479-1492 (1982).

[27] A. Stanworth and E. J. Naylor, "Polarized Light Studies of the Cornea. I. The Isolated Cornea," *J. Exp. Biol.* **30**, 160-163 (1953).

[28] B. S. Fine, S. Fine, G. R. Peacock, W. J. Geeraets, and E. Klein, "Preliminary Observations on Ocular Effects of High-Power Continuous CO_2 Laser Radiation," *Am. J. Ophthalmol.* **64**, 209-222 (1967).

[29] B. S. Fine, S. Fine, L. Feigen, and D. MacKeen, "Corneal Injury Threshold to Carbon Dioxide Laser Radiation," *Am. J. Ophthalmol.* **66**, 1-14 (1968).

[30] N. A. Peppers, A. Vassiliadis, K. G. Dedrick, H. C. Chang, R. R. Peabody, H. Rose, and H. C. Zweng, "Cornea Damage Thresholds for CO_2 Laser Radiation," *Appl. Opt.* **8**, 377-381 (1969).

[31] A. S. Brownell and B. E. Stuck, "Ocular and Skin Hazards from CO_2 Laser Radiation," Proc. 9th Army Science Conf. (1974).

[32] D. E. Egbert and E. F. Maher, *Corneal Damage Thresholds for Infrared Laser Exposure: Experimental Data, Model Predictions, and Safety Standards,* U.S.A.F. School of Aerospace Medicine, Brooks AFB, SAM-TR-77-29 (1977).

[33] E. S. Beatrice and B. E. Stuck, "Ocular Effects of Laser Radiation: Cornea and Anterior Chamber," *AGARD Lect. Ser.* **79**, 5 (1975).

[34] D. L. Van Horn and R. A Hyndiuk, "Endothelial Wound Repair in Primate Cornea," *Exp. Eye Res.* **21**, 113-124 (1975).

[35] H. C. Chang and K. G. Dedrick, "On Corneal Damage Thresholds for CO_2 Laser Radiation," *Appl. Opt.* **8**, 826-827 (1969).

[36] C. B. Bargeron, R. A. Farrell, W. R. Green, and R. L. McCally, "Corneal Damage from Exposures to Infrared Radiation: Rabbit Endothelial Damage Thresholds," *Health Phys.* **40**, 855-862 (1981).

[37] C. B. Bargeron, R. L. McCally, and R. A. Farrell, "Calculated and Measured Endothelial Temperature Histories of Excised Rabbit Corneas Exposed to Infrared Radiation," *Exp. Eye Res.* **32**, 241-250 (1981).

[38] R. L. McCally, C. B. Bargeron, W. R. Green, and R. A. Farrell, "Stromal Damage in Rabbit Corneas Exposed to CO_2 Laser Radiation" *Exp. Eye Res.* (in press).